PHOENICS News

CHAM

Dear Reader

We have a full and interesting Summer Newsletter. Thank you to all who contributed and may all reading it enjoy that activity as much as we have enjoyed compiling this edition.

Inside you will find a brief description of PHOENICS-2021 which is planned for release in early August. If you are a maintained PHOENICS User please make contact to obtain your update. If you would like to try the latest version of the software please contact phoenics@cham.co.uk.

Work is progressing to create PHOENICS on the Cloud. Please see an update on page 9.

The first online User Meeting, for Dutch and German Users, was held on June 10 and was arranged by CHAM agent Frank Kanters of Coolplug BV. Copies of some of the presentations should be available on the CHAM website soon.

Our Autumn Newsletter is in production and will be devoted to "PHOENICS at 40". The original, and first, commercially available Computational Fluid Dynamics (CFD) software - created by Professor Brian Spalding and his team - was released in October 1981. We have received contributions already from those who remember the code launch, have used PHOENICS, still use PHOENICS, work at CHAM, used to work at CHAM, etc. If you have memories you would like to share, please send them (in word format &, preferably, with a photo of yourself) to news@cham.co.uk. Thank you.

We hope you all remain well. Please get in contact if you need help, or support, with PHOENICS, FLAIR, RhinoCFD, would like some consulting work undertaken, have technical queries, or would like to trial our software and services.

Kind Regards,
Colleen Spalding
Managing Director

This Edition includes:

Summer 2021

Flow at a Rotating Disc, by Timothy Brauner and Mike Malin, CHAM, London.

Introduction

In order to obtain solutions to the Navier-Stokes (NS) equations one must use numerical methods for non-linear partial differential equations, such as those provided by PHOENICS. There are, however, some special cases of the NS equations for which exact solutions exist. These serve as excellent validation cases for numerical methods.

One such exact solution is for the steady, axisymmetric flow generated by a flat, infinite disc rotating in a quiescent fluid, sometimes also referred to as von Kármán swirling flow. Von Kármán [1] provided an analytical solution for this case by using a similarity transformation to reduce the NS equations to a set of ordinary differential equations with appropriate boundary conditions.

The rotating free disc has important practical significance because it is a limiting case of rotor-stator configurations often encountered in turbomachinery applications. It is studied here, to validate PHOENICS, as part of a wider, technical-support inquiry concerned with modelling transient, three-dimensional turbulent flow associated with a disc rotating in a housing only partially covering the disc.

Flow Description

The disc is rotating at a constant angular velocity ω about the axis originating from its centre and perpendicular to the plane in which it lies. Due to the no-slip condition on the fluid next to the disc and the effects of viscosity, a layer of fluid is swept along by the disc's rotation. The fluid is driven outwards by the centrifugal force and therefore, to conserve mass, fluid must be drawn down towards the disc from above. This is illustrated by a 3d streamline plot shown in Figure 1, where the streamlines are coloured by fluid velocity. They show that the slow (blue) fluid above is drawn towards the disc, then in the boundary layer the flow accelerates with the disc (yellow, red) while being pushed radially outward and beyond the edge of the disc (green). Figure 1 only serves for illustration purposes, because in the simulations, rotational symmetry is exploited so as to carry out the CFD analysis using a 2d axisymmetric solution domain with swirl.
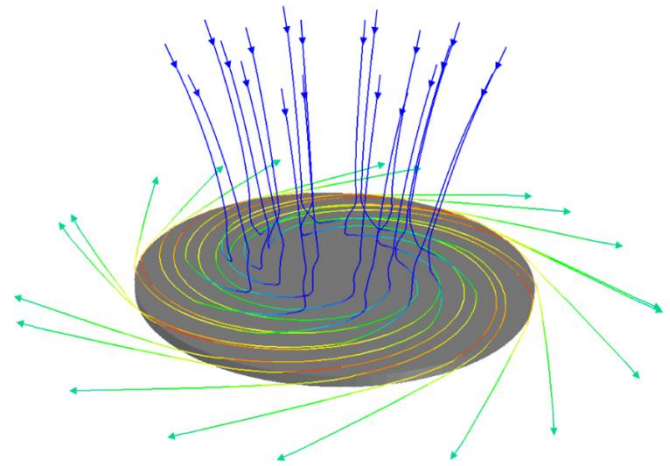

Figure 1 - Flow induced by a rotating disc in a fluid at rest. Streamline colours indicate fluid velocity.

Problem Specification

The flow is characterised by the Rotational Reynolds number Re = $\omega*R^2/\nu$, where ω is the angular velocity, R the radius of the disc and ν the kinematic viscosity. Above a certain value of Re, typically Re = $3*10^5$, the flow will undergo transition to turbulence. It should be noted that Von Kármán's results can also be applied to a disc of finite radius, under the assumption that the radius is large compared to the thickness of the fluid boundary layer on the disc [2].

As a precursor to turbulent studies, a Reynolds number of Re = $2.7*10^4$ is considered for which von Kármán's similarity solution is given in terms of the velocity scale, V = $\omega*R$, and length scale $\delta \approx \sqrt{(\nu/\omega)}$. The working fluid is air (ν = $1.544*10^{-5}$ m^2/s), the radius of the disc is R = 0.2 m and the angular velocity is ω = 10.472 s^{-1} (= 100 rpm). An angular sector of the disc of size θ = 0.1 radians is studied in detail using a polar grid with a resolution of 120 by 100 cells in the radial and axial directions, respectively. Cyclic conditions are applied in the circumferential direction. The height of the domain is 0.01 m. The radius of the domain is R_D = 0.24 m, i.e. there is a gap between the disc and the free outer boundary. Figure 2 shows the computational domain with a contour plot of velocity magnitude and corresponding vectors. The brown plane represents the sector of the disc.
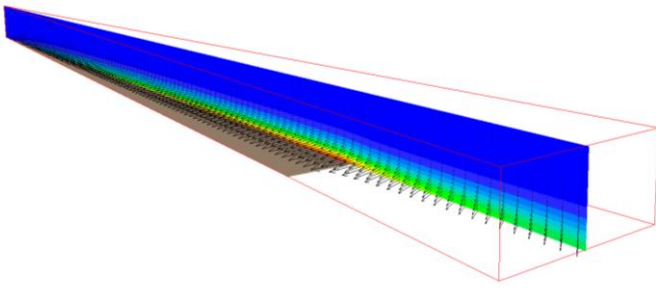
Figure 2 - Computational domain of the simulation and the sector of disc shown in brown. Slice of data showing velocity magnitude and corresponding vectors.

Results and Discussion: The velocity distribution

Von Kármán introduced the following dimensionless velocity components U, V & W, which correspond to the tangential, radial and vertical directions

$$U=G=u/(\omega r); V=F=v/(\omega r); W=H = w/\sqrt{(v\omega)}$$

where r is the local radius. It should be mentioned that U, V and W correspond to the variables G, F and H, respectively, in von-Karman's similarity solution [2]. The dimensionless velocity variables are functions of a dimensionless distance normal to the wall $\zeta = z/\delta = z\sqrt{(\omega/v)}$ [2], and they were computed in PHOENICS by using the In-Form facility. Under the assumptions of steadiness, rotational symmetry and constant angular velocity, Von Karman's normalisation results in normalised velocities being independent of the angular velocity. Consequently, the curves plotted in Figure 3 are the same for all angular velocities.
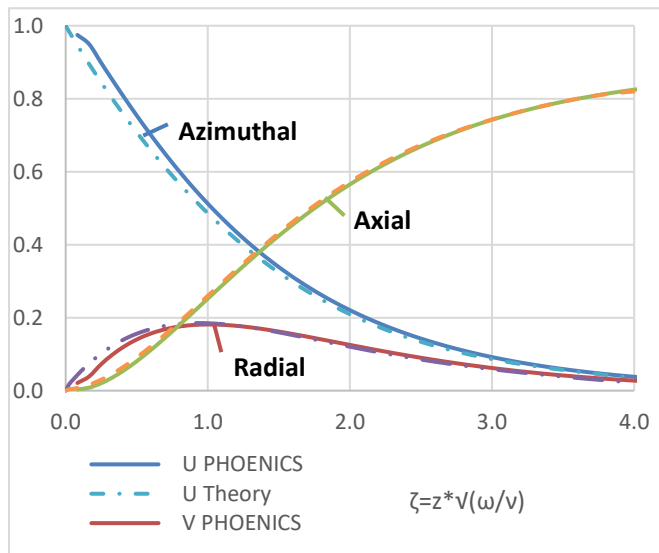

Figure 3 - Velocity distribution at a rotating disc in a fluid at rest against dimensionless wall-normal distance. Solid lines correspond to the solution computed in PHOENICS, dashed lines correspond to theory.

Figure 3 compares PHOENICS and analytical solutions for the azimuthal, radial and axial velocities. Considering only a small sector of the disc, PHOENICS matches the results of von Kármán well for each of the velocity components. Small discrepancies may arise from the finite nature of the problem studied in PHOENICS. A larger solution domain effected moving the open boundaries further from the disc, could possibly improve the results further.

The turning moment and the outward pumping flow due to centrifugal action

Additionally, two characteristic values can be investigated for a disc with finite radius: Moment/torque (M) of the disc and the volume flux (Q) of the downdraft. The moment of a disc wetted on one side is computed by integrating the circumferential component of the wall shear stress over the area of the disc [2]. The volume flux is computed by integrating the outward radial velocity over the cylindrical area surrounding the disc, or the downward axial velocity on the boundary above the disc. Table 1 provides a comparison of the analytical and PHOENICS solutions for the moment, the dimensionless moment coefficient (c_M) and the volume flux (Q).

	Theory [2]	PHOENICS
M	$2.451 * 10^{-4}$	$2.447 * 10^{-4}$
c_M	$2.350 * 10^{-2}$	$2.345 * 10^{-2}$
Q	$1.414 * 10^{-3}$	$1.414 * 10^{-3}$

Table 1 - Comparison of characteristic values from theory and numerical approximation.

Computed values for the moment and moment coefficient are in good agreement with the theory. The volume flux, derived from the mass flux through the boundary above the disc (with the same radius as the disc), is in particularly good agreement with theory.

Moment coefficient and volume flux - Reynolds-number dependence

The moment coefficient is found to be a function of Reynolds number, and is given in [2] as $c_M = 3.87/\sqrt{Re}$. When running additional simulations for various Reynolds numbers, each moment coefficient should fall on the line of c_M. This is shown in Figure 4, for three Reynolds numbers: 5000, 10000 and 27100, where the simulations are in good agreement with the theory.
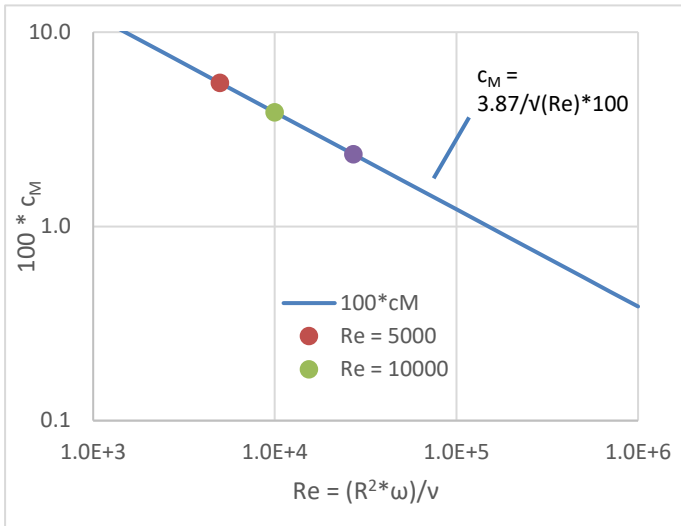
Figure 4 - Moment coefficients for a rotating disc wetted on both sides. Simulation coefficients are computed from single sided model setups.
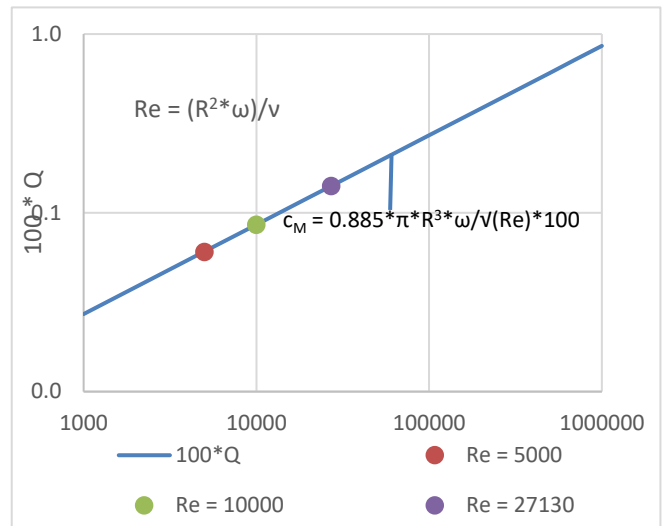

Figure 5 - Volume flux for a rotating disc wetted on one side.

The volume flux for the same Reynolds numbers is shown in Figure 5, with the equation for Q given in [2] as $Q = 0.885*\pi*R^3*\omega/\sqrt{Re}$.

Table 2 summarises the results for three different Reynolds numbers (including the results of Table 1.)

		Theory [2]			PHOENICS		
		M	c_M	Q	M	c_M	Q
Re	5000	$1.939*10^{-5}$	$5.473*10^{-2}$	$6.071*10^{-4}$	$1.939*10^{-5}$	$5.472*10^{-2}$	$6.042*10^{-4}$
	10000	$5.485*10^{-5}$	$3.870*10^{-2}$	$8.586*10^{-4}$	$5.475*10^{-5}$	$3.863*10^{-2}$	$8.565*10^{-4}$
	27100	$2.451*10^{-4}$	$2.350*10^{-2}$	$1.414*10^{-3}$	$2.447*10^{-4}$	$2.345*10^{-2}$	$1.414*10^{-3}$

Conclusions

PHOENICS has been applied to simulate the classical case of the three-dimensional, laminar boundary-layer produced by a rotating flat disc. Predictions showed good agreement with von- Kármán's analytical solution over a wide range of Reynolds numbers. This successful validation of PHOENICS allows progression to the next phase of the inquiry, which involves turbulent flow, by increasing the disc rotation speed. Then, more complex geometries will be considered where the disc can rotate in various types of housing. The present case, and those produced by further studies, will be made available in the PHOENICS Input Library of Case Examples.

References

[1] Kármán, Th. von (1921). Über Laminare und Turbulente Reibung. ZAMM. Z. Angew. Math. Mech., Bd. 1, 233–252. English translation: On Laminar and Turbulent Friction. NACA-TM-1092.

[2] Schlichting, H., & Gersten, K. (2017). Boundary-Layer Theory, Springer Berlin Heidelberg. doi:10.1007/978-3-662-52919-5

Introduction

Knowledge of the effects of an underwater explosion is important both for military and civil applications. Typically an underwater explosion starts with a rapid chemical reaction which creates gas at high pressure and temperature. This expanding gas bubble creates a shock wave which advances into the water at high speed. The bubble pressure reduces past the ambient pressure as it expands, at which point it contracts producing successively smaller bubble pressure pulses. Modelling all aspects of this process is very complicated as it involves a moving gas/water interface. The propagation of the shock wave, however, represents an important but more straightforward part of this process and it is this aspect which will form the basis of this article.

Modelling fundamentals

To model the shock propagation in water, the equation of state relating the water density to pressure, temperature and salinity is required. This can be obtained from Ref 1. A more explicit relation for density solely as a function of pressure, p, is referred to as the Tait equation, Ref 2,

$$\rho = \rho_w (\frac{p}{B} + 1 - \frac{A}{B})^{\frac{1}{\gamma}}$$

where the reference density ρ_ω is 1000 kgm^{-3} and A, B have values of 10^5 Pa and 3.31×10^8 Pa respectively and $\gamma = 7.15$. Either relation then gives the speed of sound, c as,

$$c^2 = (\frac{\partial p}{\partial \rho})_s$$

Typically the sound speed in water is about 1500ms^{-1} under ambient conditions but increases to much larger values at the very high pressures encountered in underwater explosions. Applying conservation of mass and momentum across the narrow region of a shock wave gives shock speed U (ms^{-1}) in terms of pressure and density (Ref 3),

$$U^2 = \frac{(p_m - p_A)\rho_m}{(\rho_m - \rho_A)\rho_A}$$

where suffix A represents the ambient conditions ahead of the shock and suffix m the conditions immediately downstream of the shock.
The flow speed u_m behind the shock can also be obtained as (Ref 3)

$$u_m = \frac{(p_m - p_{A)}}{\rho_A U}$$

In particular, by specifying a range of pressure jumps across the shock, the above relations can be used to determine the shock U and flow u_m speeds as functions of p_m. A useful check is to compare these results with those of Ref 4. This is done in Figure 1 (using the Fofonoff relation - similar results are obtained with the Tait equation) and shows very good agreement.
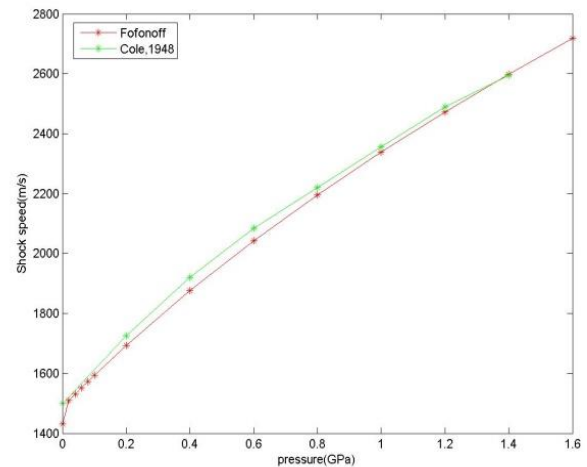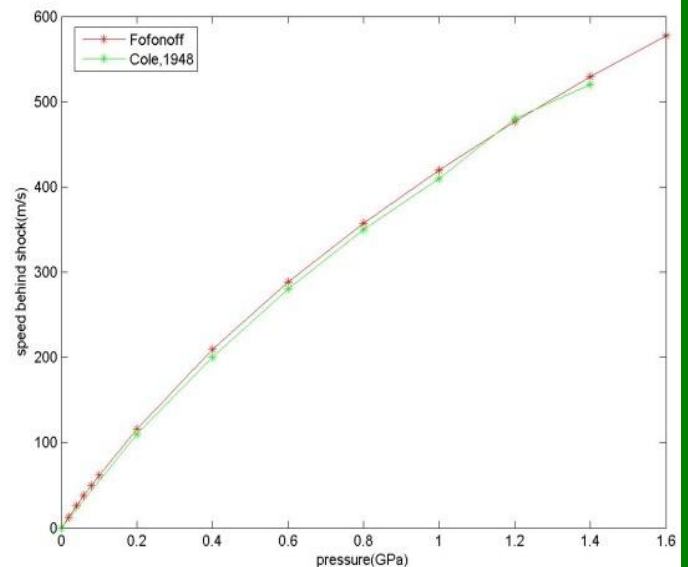

Figure 1. Comparisons of calculated shock speed (top) and fluid speed (bottom) behind shock with those of Cole, Ref 4.

PHOENICS Modelling

The simplest case to analyse with PHOENICS is that shown on the top section of figure 2. A tube of length 200m has high pressure water (4×10^8 Pa) on the left separated from low pressure water (10^5 Pa) on the right by a thin membrane. For this case both water temperatures are assumed to be the same (14C). At time t=0s the membrane is ruptured. This results in a classic 'shock tube' flow with a shock advancing to the right and an expansion wave to the left. This is analysed by PHOENICS as a 1-D compressible, time dependent flow, solving conservation equations for mass momentum and energy together with the relation defining the density as a function of pressure.

Figure 3. Pressure plots at equally spaced time intervals allowing calculation of shock and expansion wave speeds.
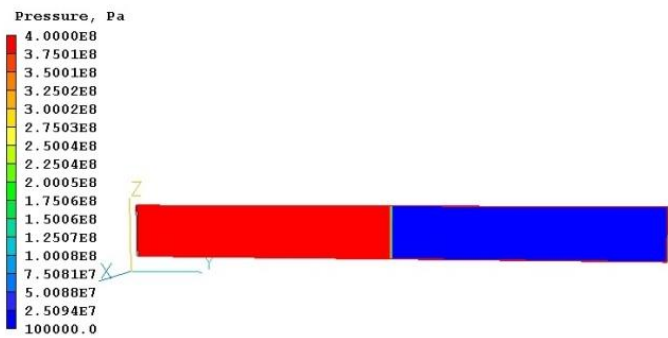

Figure 2. Top: initial setup for the first simulation with high pressure water (red) to the left and low pressure water to the right (blue). Bottom: A short time after rupture of the separating membrane.

The result of the simulation a short time after the membrane rupture is shown on the bottom section of figure 2 clearly visible in the pressure contours is the shock wave advancing to the right and the expansion wave to the left. Figure 3 shows the pressure plots at known times during the simulation. From these plots the shock speed and the speed of the expansion wave (travelling at the local sound speed) can be calculated. These values can then be compared to those calculated from the equations given above. Figure 4 shows that the comparisons are very good both for the Fofonoff and Tait density relations.
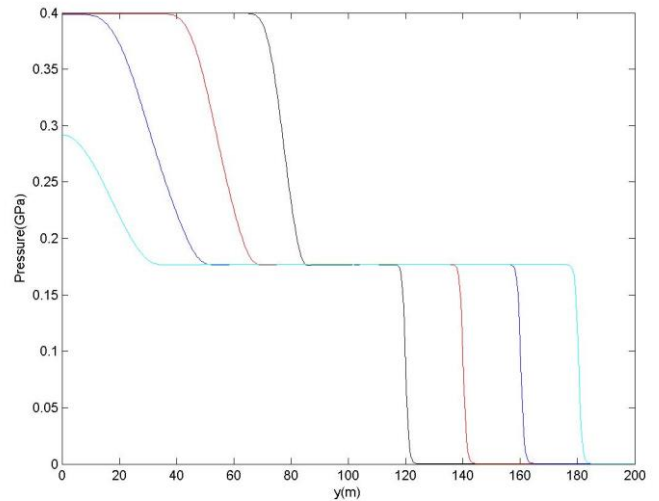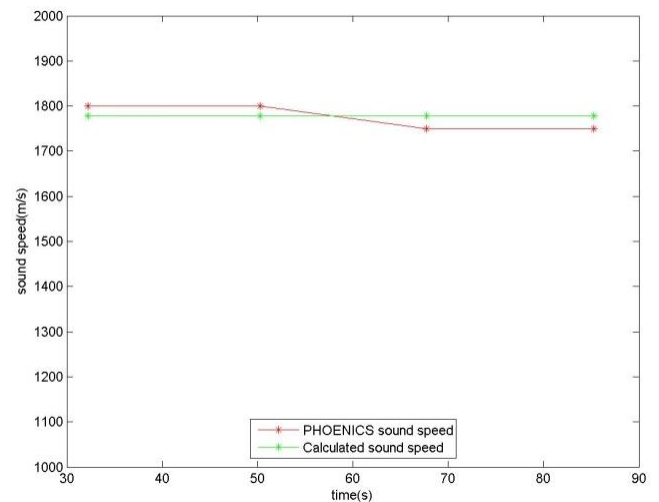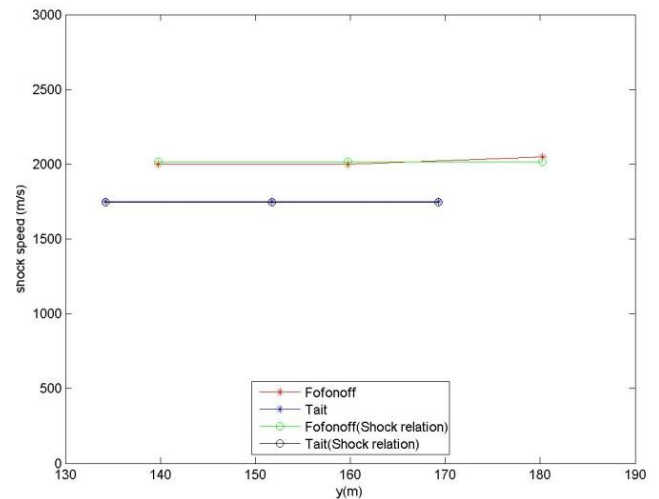

Figure 4. Comparison of shock (top) and expansion wave (bottom) speeds with those calculated from the PHOENICS results.

6

The most common explosives in experiments at sea are 0.82kg SUS (Signal, Underwater Sound) charges that are comprised principally of TNT. Empirical relations based on sea trials have been given by Chapman (Ref 5) for the peak shock pressure p_m as a function of charge weight, w (kg), and range R(m),

$$p_m = 10^6 x 50.94 (\frac{w^{\frac{1}{3}}}{R})^{1.13}$$

The exponential decay of pressure after passage of the shock is given by,

$$p = p_m \exp(-t/\tau_s)$$

where the time constant is given by,

$$\tau_s = 8.12 x 10^{-5} w^{\frac{1}{3}} \left(\frac{w^{\frac{1}{3}}}{R}\right)^{-0.14}$$

If these relations are assumed to hold in the initial stages of the gas bubble and shock formation, this pressure time variation can be fixed in the relevant PHOENICS cell(s) to allow a simplified simulation of an explosive charge. The results from an axisymmetric simulation with a 0.82kg SUS charge placed at the centre of a 10m radius domain are shown in Figure 5. The shock speed at t=0.003s (top section of Figure 5) is approximately 1700 ms-1 with pressure reducing inversely with distance from the centre. The pressure plots at equally spaced time intervals are shown on the bottom section of
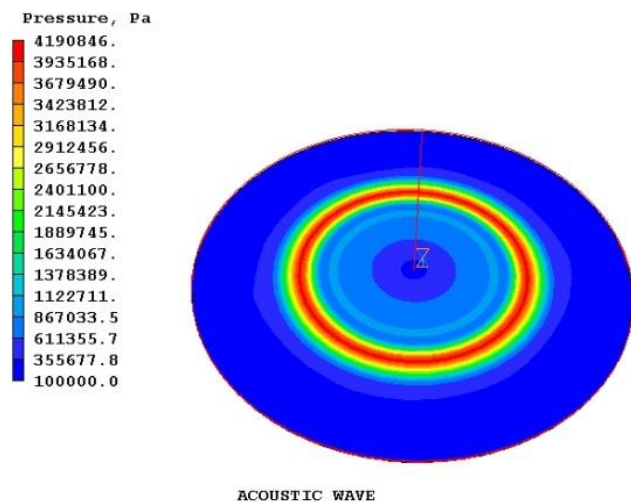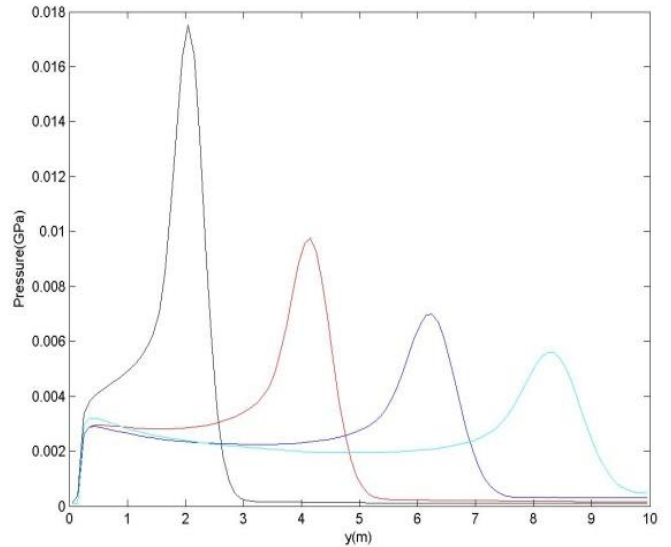

Figure 5: Pressure contours showing shock wave after detonation of explosive charge.

Pressure plots at equally spaced time intervals.

Conclusion

The results above show that either the Fofonoff or Tait equations relating water density to pressure can work well with PHOENICS in simulating underwater shock propagation or, more generally, sound propagation in water.

References

1. Fofonoff N P, Physical Properties of Seawater: A New Salinity Scale and Equation of State for Seawater, J Geophys Res vol 90, p3332 (1985).

2. Li Y H, Equation of state of water and seawater, J Geophys Res 72, 2665-2678 (1967).

3. Medwin H, Clay C S, Fundamentals of Acoustical Oceanography, Academic Press (1998).

4. Cole R H, Underwater Explosions, Princeton University Press, Princeton, N J, (1948).

5. Chapman N R, Measurement of the waveform parameters of shallow explosive charges, The Journal of the Acoustical Society of America, 78, 672 (1985).

Dr R P Hornby, bob.hornby007@gmail.com

All Users will benefit from the following improvements:

- Use of VBO shaders to produce better on-screen images:
- Better, smoother shading and illumination of objects, contours and iso-surfaces;
  - Display of shadows, linked to the solar position if the SUN object is active;
  - Improved transparency handling especially when multiple transparent objects overlap;
  - Optional simple drawing mode highlighting sharp edges.
- Ability to set domain origin to any arbitrary location, including in negative quadrants. Objects can be flagged 'At start' to lie always at domain origin which is not tied to (0,0,0).
- Clean-up of object geometry libraries with easier access to basic primitives simplifying construction of new models.
- Improved import of groups of CAD geometries – relative positions cannot be influenced by order of importing, and several groups can be imported preserving relative positions between them.
- When CAD objects need to be located in the negative co-ordinate quadrant, the domain origin is automatically reset to enclose the imported objects.
- Minimum and maximum exit values for temperature and solved scalars can be set for linked ANGLED_IN objects. eg for a heater exit temperature cannot exceed heating element temperature.
- The process of saving viewer animations is improved.
- A new TRACK_COUNTER object reports the number of GENTRA or Viewer streamline tracks passing through and also reports time of arrival for each track.
- Individual streamlines can be coloured.
- Contours and vectors in double-cut cells can be displayed – a vector is drawn on each side of a thin solid cutting a cell in two.
- The temperature contour display for PARSOL is improved, with better capture of the sharp temperature change at solid-fluid boundaries.

FLAIR Users will benefit from:

- Air Change Efficiency (ACE) is printed for the domain and each ROOM object, and placed in 3D store ACE. ACE is derived based on room age-of-air, and on the global domain age-of-air.

- The menu panel for activating Aerosols to prevent loss of settings for derived quantities has been corrected. However, if humidity is to be solved it must be activated before the Aerosols.

PHOENICS-on-the-Cloud:

- PHOENICS is being made available on a Pay-As-You-Go basis through the Microsoft Azure MarketPlace.
- A range of Virtual Machines will be available at competitive prices.

Improvements to the Solver

- PARSOL has been further revised to allow (optionally) for double-cut cells.
- Temperature gradients can be stored by adding STORE(DTDX,DTDY,DTDZ).

Improvements to PHOENICS used under Linux:

- The Linux version GUI looks and feels like the Windows version when run through WINE
- The native Linux solver now includes HYPRE solvers and parallel operation, as well as supporting the SUN object.

Bug Fixes Include:

- Corrections to Transfer objects in transient cases – only the transfer object for the timestep in question is written, not for all timesteps at each step.
- In parallel cases transfer-data files are written to the slave processors more efficiently, greatly speeding up the start of the calculation especially in transient cases.
- Distribution of the facetdat file to the slave processors in parallel has been improved, leading to a speed up in start-up time.
- The SUN object has been corrected to prevent inadvertent heat sources in un-illuminated cells.
- Solar heat load is added to heat balance at isothermal PLATE and THINPLT objects when the IMMERSOL or P1T3 radiation models are active.
- Transient thermal accumulation at a THINPLT object is included when the IMMERSOL or P1T3 radiation models are active.
- Multiple objects within a single ROTOR are recognised correctly after an error correction in the user-selection of objects with a ROTOR.

Work is underway to develop an offering of PHOENICS that can be run on the Azure cloud platform. It is expected that this will allow significant flexibility and rapid scaling capabilities for our users.

Preliminary testing has shown a potential for a massive speed up by leveraging the workstation - grade hardware available on the cloud that would be otherwise prohibitively expensive for many users. 120 - Core machines are available with up-to 16 memory channels; this can speed up run time by a factor of 20.

Test Cases

We carried out testing with two real world cases:

- 9 million cell case of ventilation in a car park
- 24 million cell case of flow in a city sized environment

The following increased speeds were observed when running on a high - core - count system:

Scaling of cases on HB120v2 by cell and processor count
(higher is better)
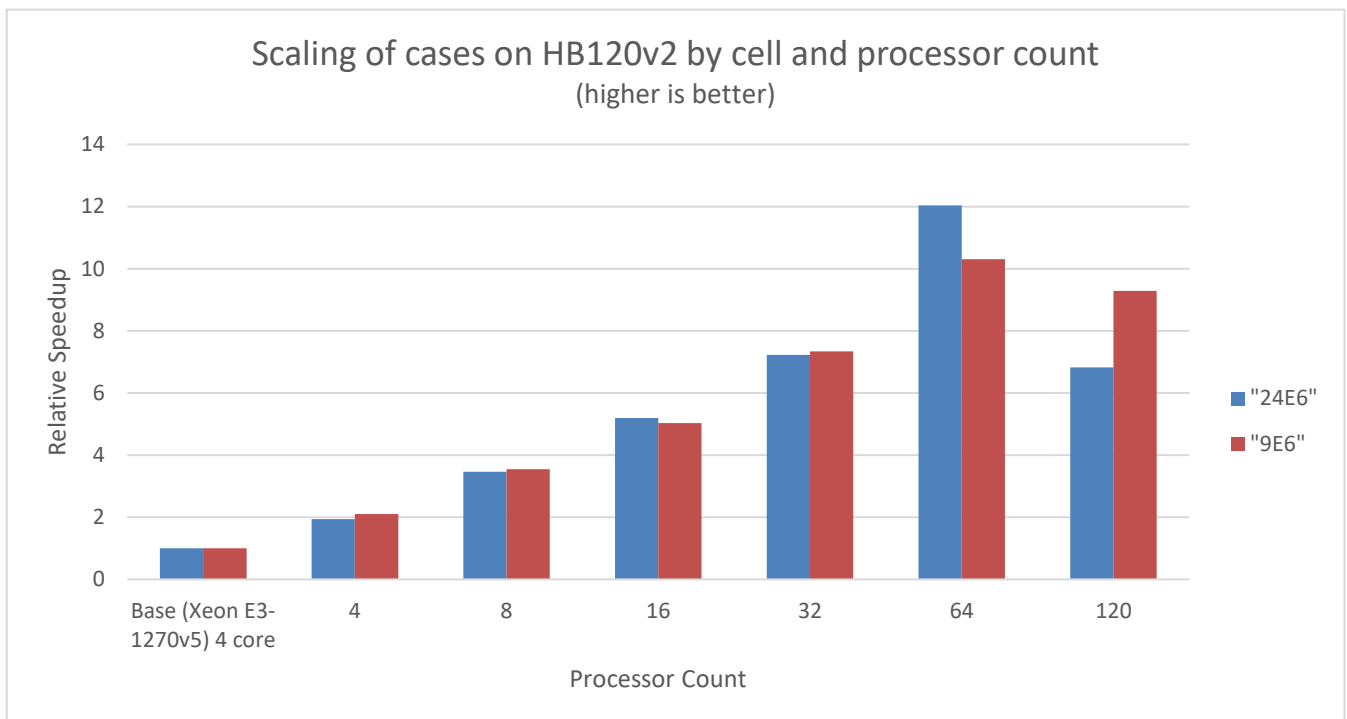
System Specifications

Test results are normalized using test scores of a Xeon E3-1270v5 system. This is a 4 - core system compatible with DDR4 (two channel) memory. This computer system was chosen as these specifications are common among many standard office computers.

The system used for testing is an AMD EPYC 7002 (dual socket configuration) with a total of 120 available cores and a total of 16 DDR4 memory channels due to dual socket configuration.

Implications for Project Timing

Our investigation found that running a simulation that would take 20 days on limited hardware, or 5 days on a reasonable Threadripper PC, can now be done, problem free, in under two days to meet tight deadlines.

(https://www.broadberry.co.uk/high-performance-workstations/cyberstation-amd-epyc-pro)

Performance testing showed that users can get the best results when running a 64 core configuration or running multiple cases simultaneously to get a better overall value for money.

Scaling when running multiple cases
(lower is better)

Relative Time (9E6 case)

Processor Count	Relative Time
64 core - single case	1.0
60 core - 2 case parallel * 2	2.8
64 core - 4 cases in sequence	4.0
30 core - single case	1.4
30 core - 4 cases in parallel	2.9
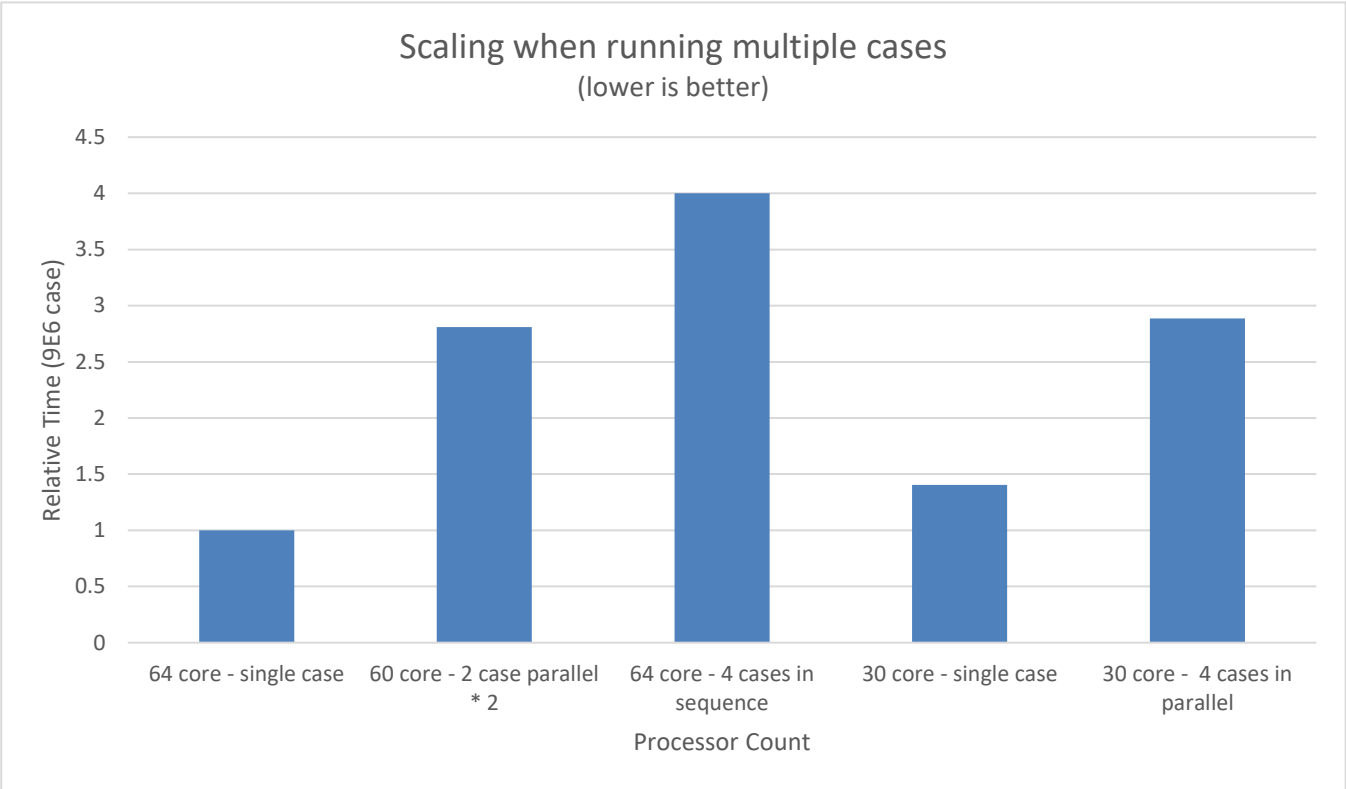
The above data show that a 120 core VM can provide quick results for single cases. Running 2 cases on 60 cores each, or 4 cases on 30 cores each concurrently, means 4 cases run faster than 1 case on 64 cores sequentially. This allows for cost savings of over 25% when running multiple variations of a simulation.

News from CHAM Agents: GERMAN PHOENICS USERS MEETING – JUNE 2021

COOLPLUG

As a result of the restrictions imposed by the on-going COVID pandemic, CHAM's agent - Frank Kanters of Coolplug BV - hosted the first, on-line, PHOENICS User Meeting for a group of his customers selected from the German & Dutch user base. The two-hour event, held on 10th June, featured:

BIM-related presentations by Dr Eckehard Fiedler from a long-standing PHOENICS user, Krantz GmbH;

Phoenics for BIM

Dr.-Ing. Eckehard Fiedler

Selected images from a COVID-release-in-an-arena scenario by Coolplug, on behalf of Zimmermann & Becker GmbH;
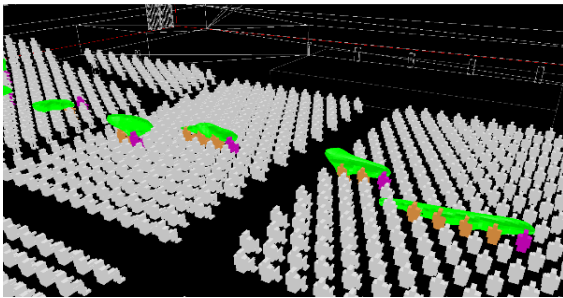

Image shows the path of the aerosols as isosurfaces from the emitter (red) to the receiver (yellow) in the parquet in front of the stage

Advice from David Glynn on the use of FLAIR's inbuilt features for modelling wind, rain, pedestrian comfort and evapotranspiration from foliage.
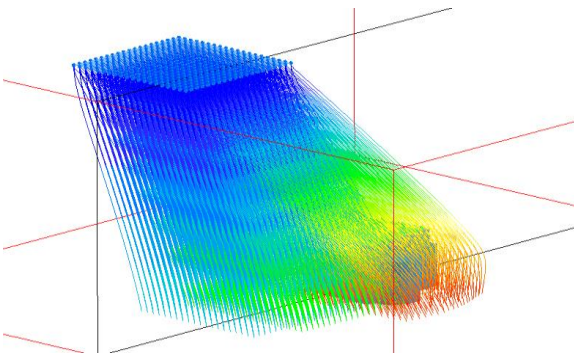

Image shows the wind-driven rain tracks from the rain object and impinging upon a building

A primary aim of the Meeting was to inform users of major features of the PHOENICS-2021 release. The presentation, made by John Ludwig, covered topics such as the shading improvements offered by implementing VBO graphics, and local unstructured grids created by the updated PARSOL cut-cell treatment using new solvers introduced in PHOENICS.
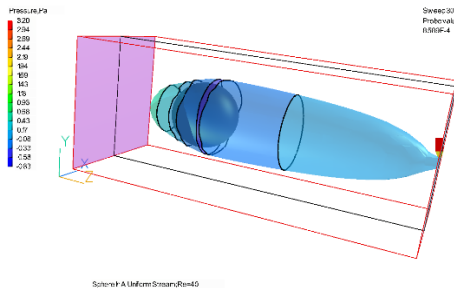
CHAM took the opportunity to announce the forthcoming availability of *"PHOENICS on the Cloud"* which will permit customers to access PHOENICS from anywhere in the world without the need to download a copy. It also enables the current PHOENICS user base to outsource very large simulations to run on the powerful, multi-core systems offered by Microsoft's Azure Cloud service.

PHOENICS-2021 features can be found in the updated "What's New in PHOENICS" document at:
http://www.cham.co.uk/phoenics/d_polis/d_docs/tr006/tr006.pdf

The on-line User Meeting format proved successful - at least for a relatively small group such as that involved on this occasion - and will be adapted for similar customer events and on-line Training Courses.

- May 17, 18, 19 Shanghai-Feiyi exhibited PHOENICS at the 17th International Conference on Green and Green and Energy Efficient Building and New Technologies and Products Expo.
- May 22, 23 Shanghai-Feiyi exhibited PHOENIS at the 6th National Youth Combustion Academic Conference (In Hangzhou)
- May 28, 29 Shanghai-Feiyi exhibited PHOENICS at NVCT 2021 National Acoustics Engineering Technology Summit Forum (in Hangzhou.)

Contact Us:

Should you require any further information regarding our products or services please give us a call on +44 (20) 89477651; alternatively you can email us on sales@cham.co.uk.

Visit our website at www.cham.co.uk; we are also on the following social media sites: